Molecular Dynamics Simulation Study of Heat Transfer Across Solid-Fluid Interfaces in a Simple Model System

Sebastian Schmitt, Truong Vo, Martin P. Lautenschlaeger, Simon Stephan, and Hans Hasse[a)]

Laboratory of Engineering Thermodynamics (LTD), TU Kaiserslautern, Kaiserslautern 67663, Germany

(Dated: 2022-04-23)

Nanoscale heat transfer across a solid-fluid interface was investigated by molecular dynamics simulations. The studied system consists of a fluid confined between two parallel plane atomistic walls. There is no convection. Both the fluid and the solid were modeled with the Lennard-Jones truncated and shifted potential. The following parameters were varied systematically: strength of solid-fluid and solid-solid interaction, mass of solid particles, temperature difference between fluid and solid, fluid temperature, fluid density, and channel width. From the simulation results, numbers for the Kapitza length L_K were obtained, which characterizes the heat transfer resistance at the solid-fluid interface. A correlation of the results for the Kapitza length L_K as a function of the studied variables was developed. A dimensionless number is introduced, the Kapitza interface number Ki, which describes the Kapitza effect in the stagnant fluid and is zero in the absence of the Kapitza effect. It is known that the heat transfer resistance at the interface is generally not influenced by convection, such that the results from the present work can also be used to describe heat transfer with convection in cases in which the Kapitza effect plays a role, or simply to assess the influence of the Kapitza resistance.

[a)]Electronic mail: hans.hasse@mv.uni-kl.de

I. INTRODUCTION

The heat transfer across solid-fluid interfaces plays an important role in many technical and natural processes. For describing macroscopic heat transfer, it is generally sufficient to assume that thermal equilibrium is established at the interface. As dimensions get smaller, surface phenomena become increasingly important and interfacial effects begin to play a significant role. This work deals with the interfacial effects associated with heat transfer that were systematically studied first by Pyotr Leonidovich Kapitza[1].

The heat transfer between a solid and a fluid phase requires energy transfer between the particles in the solid and those in the fluid. There is a heat transfer resistance associated with this, which is known as Kapitza resistance R_K[2] and often expressed in terms of the Kapitza length L_K[3]. In heat transfer theory, the Kapitza length L_K plays a similar role as the slip length L_S in fluid dynamics, which replaces on the microscale the assumption of zero slip used for describing macroscopic flow processes. In macroscopic heat transfer theory, the Kapitza resistance is usually neglected and replaced by the assumption of thermal equilibrium between both phases at the interface.

The Kapitza resistance is difficult to study experimentally. Therefore, molecular dynamics (MD) simulations have been frequently used in the literature to study its influence on heat transfer[3–11]. The available results show that the Kapitza resistance plays an important role in heat transfer on the nanoscale. Notably, there is a temperature jump at the interface, which has to be accounted for and which is directly related to the Kapitza length L_K. The Kapitza resistance at solid-fluid interfaces of many material pairings has been studied by NEMD simulations[12–15], often with water as fluid component[16–18]. Besides the variation of the material pairings, the influence of single simulation parameters like the channel width[19,20], the surface geometry[13,21], the temperature or the thermostating[17,22–24], the fluid density[25,26], and the solid-fluid[4,9,10,18,27–29] as well as the solid-solid interaction[3,6,30,31] were determined by MD simulations.

While numbers for L_K have been determined for various situations, no relations have been established yet that allow an estimation of L_K for a wide range of conditions. We have therefore carried out a comprehensive MD study of the Kapitza resistance for a model system for which different influencing parameters were varied systematically and used the results for establishing an empirical correlation.

The simulation scenario used in the present work consists of a fluid confined between two parallel fixed plane walls: a hot and a cold one. There is no convection. Both the fluid and the walls were modeled with the Lennard-Jones potential truncated and shifted at the cut-off radius $r_c^* = 2.5\ \sigma$ (LJTS). This potential is well studied regarding both bulk[32–34] and interfacial properties[35–41] and is often used to study processes on the nanoscale[42–46]. Moreover, the LJTS potential provides a simple yet realistic model for simple spherical substances[47]. The effects of different influencing factors (solid-fluid interaction, solid-solid interaction, mass of the solid particles, temperature difference between fluid and solid, fluid temperature, fluid density, and channel width) on the heat transfer between the walls and the stagnant fluid were thereby studied systematically. Based on these results, an empirical correlation was developed in this work that describes the heat transfer resistance at the interface as a function of those influencing factors. Furthermore, a dimensionless number is introduced, which we call Kapitza interface number Ki, to distinguish it from the well-known Kapitza number Ka[48]. The latter describes the flow of a fluid down an inclined surface, another phenomenon that has been studied by Pyotr Leonidovich Kapitza. The Kapitza interface number Ki relates the Kapitza length L_K to a characteristic macroscopic length of the heat transfer problem, called H here, i.e. $Ki = L_\mathrm{K}/H$. It is straightforward to show that Ki can be interpreted as the ratio of the Kapitza resistance R_K and the heat transfer resistance due to heat conduction in the fluid R_cond, i.e. $Ki = R_\mathrm{K}/R_\mathrm{cond}$. If the characteristic macroscopic length H is large, Ki goes to zero and the Kapitza resistance becomes much smaller compared to the conductive resistance.

Surprisingly, there are only few studies available in which the interfacial heat transfer on the microscale was related to that on the macroscale[49,50]. In the presence of convection, the macroscopic heat transfer is usually described by the Nusselt number Nu. Formally, the Nusselt number can also be applied when there is no convection. This results in $Nu = 1$[51], if the usual definition is applied. The interfacial heat transfer resistance reduces that number[49,50], but as dimensions increase, the limit of $Nu = 1$ is finally attained, as long as there is no convection. It has been shown that the interfacial heat transfer resistance is hardly influenced by convection, even for large streaming velocities[49], such that results obtained for stagnant conditions, as those reported in the present work, can also be used for estimating the heat transfer conditions if convection is present.

This paper is organized as follows: first, details on the molecular model are given. Then,

the MD simulation setup and sampling procedure for the observables are presented. Furthermore, the dimensionless quantities used are introduced and an overview of the set of simulations that were carried out is presented. In the subsequent section, the results are reported including a discussion of the effect on the molecular level. Then, the correlation describing the heat transfer based on the simulation data is presented and it is shown how that can be applied in also more complex heat transfer problems. Finally, conclusions are drawn.

II. MOLECULAR MODEL

All molecular interactions were modeled using the LJTS potential, which is based on the Lennard-Jones (LJ) potential:

$$u^{\mathrm{LJTS}}(r_{ij}) = \begin{cases} u^{\mathrm{LJ}}(r_{ij}) - u^{\mathrm{LJ}}(r_c) & r_{ij} < r_c \\ 0 & r_{ij} \geq r_c \end{cases} \tag{1a}$$

$$u^{\mathrm{LJ}}(r_{ij}) = 4\varepsilon \left[\left(\frac{\sigma}{r_{ij}} \right)^{12} - \left(\frac{\sigma}{r_{ij}} \right)^{6} \right] \quad , \tag{1b}$$

where r_{ij} is the intermolecular distance between two particles i and j, σ is the size parameter, and ε is the energy parameter. The truncation radius is $r_c = 2.5$ for all molecular interactions and in all simulations of the present work.

All size parameters are the same: $\sigma_{\mathrm{ff}} = \sigma_{\mathrm{ss}} = \sigma_{\mathrm{sf}} = 1$, where "ff" stands for interactions in the fluid f, "ss" stands for interactions in the solid s, and "sf" stands for solid-fluid interactions. The influence of the attractive solid-solid and solid-fluid interactions as well as the mass of the solid particles on the interfacial heat transfer resistance was studied systematically by varying the corresponding parameters $\varepsilon_{\mathrm{ss}}$, $\varepsilon_{\mathrm{sf}}$, and M_{s}, respectively.

All physical quantities are reported using classical reduced Lennard-Jones units, i.e. all quantities are reported with respect to the parameters of the LJTS potential of the fluid: the energy parameter $\varepsilon_{\mathrm{ff}}$, the size parameter σ_{ff}, and the mass M_{f}. The employed relations are summarized in Table I. The reduced units system obtained in this way should be distinguished from dimensionless quantities introduced to lower the number of independent parameters for describing a physical problem, such as the Nusselt number Nu or the Kapitza

interface number Ki. The latter can be formulated either directly with physical SI unit quantities or, equivalently, with the corresponding reduced Lennard-Jones unit quantities.

TABLE I. Definition of the reduced units system. The corresponding quantities carrying an SI unit dimension are marked by an asterisk. The values used for the normalization are the potential parameters of the fluid σ_{ff}, $\varepsilon_{\mathrm{ff}}$, and M_{f}.

Physical quantity	**Reduced units**
Length	$x = x^*/\sigma_{\mathrm{ff}}$
Mass	$M = M^*/M_{\mathrm{f}}$
Time	$t = t^*/(\sigma_{\mathrm{ff}}\sqrt{M_{\mathrm{f}}/\varepsilon_{\mathrm{ff}}})$
Density	$\rho = \rho^*/\sigma_{\mathrm{ff}}^3$
Energy	$u = u^*/\varepsilon_{\mathrm{ff}}$
Temperature	$T = T^*/(\varepsilon_{\mathrm{ff}}/k_{\mathrm{B}})$
Heat flux	$q = q^*/(\varepsilon_{\mathrm{ff}}/(\sigma_{\mathrm{ff}}^3\sqrt{M_{\mathrm{f}}/\varepsilon_{\mathrm{ff}}}))$
Thermal conductivity	$\lambda = \lambda^*/(k_{\mathrm{B}}/(\sigma_{\mathrm{ff}}^2\sqrt{M_{\mathrm{f}}/\varepsilon_{\mathrm{ff}}}))$
Kapitza length	$L_{\mathrm{K}} = L_{\mathrm{K}}^*/\sigma_{\mathrm{ff}}$
Kapitza resistance	$R = R^*/(\sigma_{\mathrm{ff}}^3\sqrt{M_{\mathrm{f}}/\varepsilon_{\mathrm{ff}}}/k_{\mathrm{B}})$
Heat transfer coefficient	$\alpha = \alpha^*/(k_{\mathrm{B}}/(\sigma_{\mathrm{ff}}^3\sqrt{M_{\mathrm{f}}/\varepsilon_{\mathrm{ff}}}))$

III. METHODS

A. Simulation Details

The simulation setup consists of a hot and a cold wall, which confine a stagnant fluid. A snapshot of the simulation setup is depicted in Fig. 1.

The solid walls had an FCC crystal structure and the (001) surface at the solid-fluid interface. The coordinate system used is depicted in Fig. 1: $z = 0$ indicates the initial position of the first solid layer of the hot wall that is in direct contact with the fluid. The dimensions of the box in the x- and y-direction were $\Delta x = \Delta y = 21.8$. The thickness of each solid wall in the z-direction was 14. The fluid channel width was 2 H, where H is the distance from $z = 0$ to the center of the channel. The wall position $z = 0$ was defined as the average z-position of all particles of the first layer (directly in contact with the fluid

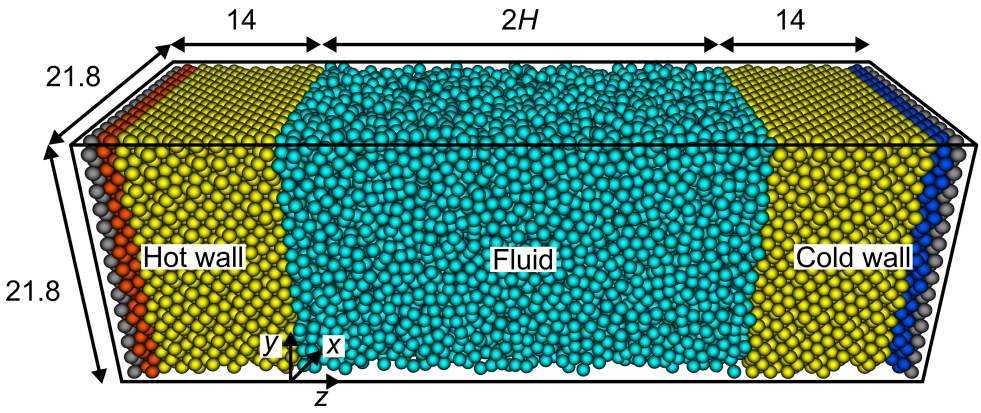

FIG. 1. Snapshot of the simulation setup. The cyan particles represent the fluid. The remaining particles (gray, red, blue, and yellow) belong to the solid walls, including two fixed layers at the boundaries in z-direction (gray particles) and two thermostatted regions next to those with T_{hot} (red particles) and T_{cold} (blue particles). The thermostats induce a temperature gradient in the channel. The yellow particles of the walls are unconstrained. The box boundaries are depicted as black lines. The dimensions of the simulation box are given. The length H is half the channel width and was systematically varied in our study.

particles) of the left wall (cf. Fig. 1). The channel width was systematically varied in our study.

Periodic boundary conditions were applied in the x- and y-directions. The two layers of the hot and the cold walls next to the fixed layers were thermostatted (red and blue particles in Fig. 1). The temperature was high in one wall (T_{hot}) and low in the other (T_{cold}). Thus, a heat flux in positive z-direction was induced and measured as described below. Due to the geometry of the setup, the temperature of the fluid in the center of the channel is approximately $T_{\mathrm{f}} = (T_{\mathrm{hot}} + T_{\mathrm{cold}})/2$.

All simulations were carried out using the LAMMPS package[52]. The simulation time step was 0.002. Each simulation run started by 1 million time steps of equilibration in the NVT ensemble. During that equilibration, a Nosé-Hoover thermostat was applied to the entire system for thermostatization to the temperature T_{f}. Subsequently, non-equilibrium conditions were prescribed for 4 million time steps, in which a Langevin thermostat was used to control the temperature in the thermostatted zones of the hot wall and the cold wall. The temperature of the walls were $T_{\mathrm{hot}} = T_{\mathrm{f}} + \Delta T_{\mathrm{w}}$ and $T_{\mathrm{cold}} = T_{\mathrm{f}} - \Delta T_{\mathrm{w}}$, where ΔT_{w} is a system parameter that was systematically varied in the study. Within that non-equilibrium

simulation phase, a steady state with a stationary temperature profile was built up during the first 1 million time steps. The following 3 million time steps were used for the sampling of the results. No drift of the total energy appeared in the sampling phase of the simulations.

The simulation volume was uniformly discretized in z-direction for the sampling of local properties. The local density and temperature were determined in bins of the thickness $\Delta z_\rho = 0.1$ and $\Delta z_T = 0.5$, respectively. An exemplaric temperature profile and a fluid density profile obtained from the simulations from the hot wall to the middle of the channel is shown in Fig. 2. There, the layering of the fluid at the wall, i.e. the adsorption layer, can be seen. The adsorption in solid-fluid dispersive systems has been extensively studied in the literature[40,41,53–58]. At the depicted state point (cf. Fig. 2), multiple layers of particles are observed in the adsorption film, which reaches approximately $z = 8$. Fluid particles at larger distances from the wall, i.e. $z > 8$ are considered as 'bulk fluid' in the following. Therefore, the smallest considered channel width in this work was chosen as $H = 10$ such that there was a small bulk region present in all cases. The uncertainty of the sampled Kapitza length L_K was calculated by block averaging. For this purpose, the sampling part of the non-equilibrium simulation phase was divided into ten blocks, each of a length of 300,000 time steps and the Kapitza length was calculated for each block. The given uncertainties are the standard deviation of the ten values. The results reported for L_K are the mean values of the ten block results.

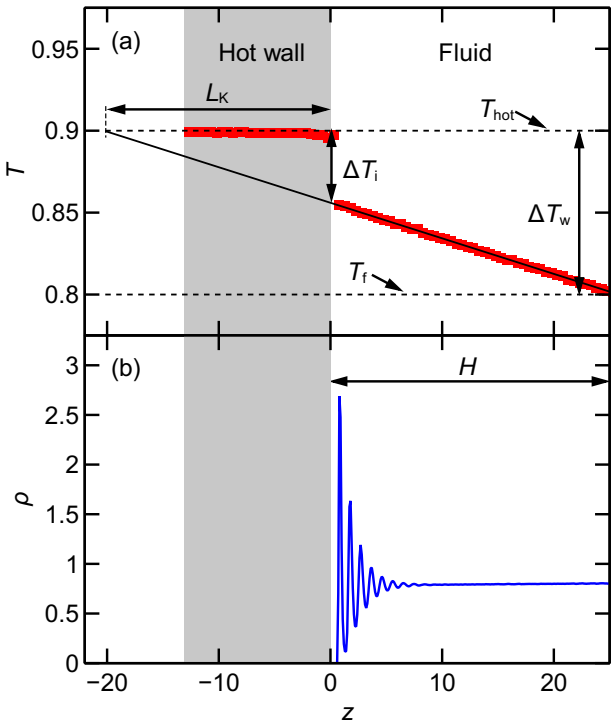

FIG. 2. Exemplaric simulation result for (a) a temperature profile in the simulation box and (b) a density profile of the fluid for the hot side of the simulation box. The wall is indicated by the gray shaded area. The black solid line in (a) is a linear fit of the fluid temperature profile. The horizontal dashed lines in (a) indicate both the temperature of the hot wall T_{hot} and the fluid temperature T_{f} (i.e. the temperature in the middle of the channel). The temperature difference at the interface ΔT_{i} and the temperature difference between the hot wall and the fluid in the middle of the channel ΔT_{w} are also depicted.

B. Theoretical Background

From the temperature profiles sampled during the simulations, the temperature jump at the interface ΔT_{i} and the Kapitza length L_{K} were determined as indicated in Fig. 2 at both the hot and the cold side. Furthermore, the heat flux q was determined from

$$q = \frac{1}{A_{\mathrm{s}}} \frac{\mathrm{d}E}{\mathrm{d}t} \,, \tag{2}$$

where $\mathrm{d}E/\mathrm{d}t$ is the slope of the cumulative kinetic energy added to the hot wall and removed from the cold wall with respect to the time (see the Supplementary Material for details) determined by linear regression and A_{s} is the cross-sectional area of the solid-fluid interface,

which was computed as the cross-section of the simulation box $A_\mathrm{s} = \Delta x\, \Delta y$.

Applying Fourier's law of heat conduction to the bulk fluid region, here to the hot side of the simulation box (cf. Fig. 2, analogously applicable to the cold side of the simulation box), yields

$$\frac{q}{\lambda} = -\frac{\mathrm{d}T}{\mathrm{d}z} = \frac{\Delta T_\mathrm{i}}{L_\mathrm{K}} = \frac{T_\mathrm{hot} - T_\mathrm{f}}{H + L_\mathrm{K}} \ , \tag{3}$$

where $\mathrm{d}T/\mathrm{d}z$ indicates the slope of the temperature profile determined from a linear fit to the sampled simulation results in the bulk fluid region (cf. Fig. 2). In Eq. (3), λ is the thermal conductivity of the bulk fluid, which is assumed to be constant in the channel. The numbers for λ were determined by the slope of the temperature of the fluid in the channel in the stationary phase and the heat transferred from the hot to the cold wall (cf. Eq. 3). The values obtained were compared to an empirical correlation from a previous work of our group[33]. Good agreement (AAD of 2.9%) of the simulated values and the empirical correlation from Lautenschlaeger and Hasse[33] in the range of validity of the correlation ($\rho_\mathrm{f} > 0.2$) was found. The uncertainty of the empirical correlation was estimated to be 2.4%[33]. The temperature jump at the interface is indicated as ΔT_i. The Kapitza length L_K can be determined either from Eq. (4a) or from Eq. (4b):

$$L_\mathrm{K} = \frac{\lambda}{q} \Delta T_\mathrm{i} \ , \tag{4a}$$

$$L_\mathrm{K} = \frac{\lambda}{q} (T_\mathrm{hot} - T_\mathrm{f}) - H \ , \tag{4b}$$

which are equivalent as long as the temperature profile in the fluid is linear, which was well satisfied by all simulation results from this work. As the statistical uncertainties were found to be smaller when L_K was determined using Eq. (4b), this route was applied in the present work.

IV. INFLUENCING FACTORS AND OVERVIEW OF THE SIMULATIONS

The following influencing factors on the heat transfer at the microscale were considered in the present work:

- the dispersion energy ε_sf describing the solid-fluid interactions,

- the dispersion energy $\varepsilon_{\mathrm{ss}}$ describing the solid-solid interactions,
- the mass of the solid particles M_{s},
- the temperature difference between the mean fluid temperature and the walls ΔT_{w},
- the mean fluid temperature T_{f},
- the fluid density ρ_{f}, and
- the channel width H.

The interaction parameters $\varepsilon_{\mathrm{sf}}$, $\varepsilon_{\mathrm{ff}}$, and $\varepsilon_{\mathrm{ss}}$ are not independent due to the reduced units system (cf. Table I), which is why $\varepsilon_{\mathrm{ff}}$ was not varied here.

TABLE II: Overview of the simulations of the present study and results obtained for the heat flux q and the Kapitza length L_{K}. The variables of the settings are described in the text. Simulation 1 is the *default simulation*. Plain entries of settings have the same value as the default simulation.

	Setting							Results	
Simulation	T_{f}	ΔT_{w}	ρ_{f}	$\varepsilon_{\mathrm{sf}}$	$\varepsilon_{\mathrm{ss}}$	M_{s}	H	q	L_{K}
1	0.80	0.10	0.80	1.00	30	2.0	10	0.01934	21.665
2	0.85		0.80					0.02011	19.638
3	0.90		0.81					0.02118	20.075
4	0.95		0.80					0.02202	17.965
5	1.00		0.80					0.02278	17.856
6	1.05		0.81					0.02436	15.850
7	1.10		0.81					0.02512	15.216
8	1.20		0.81					0.02613	13.798
9	1.30		0.80					0.02792	13.032
10			0.81	0.25				0.00554	105.270
11			0.81	0.50				0.01000	51.330
12			0.80	0.75				0.01441	31.112

13		0.81	1.25			0.02299	16.434
14		0.80	1.50			0.02554	12.891
15		0.80	1.75			0.02773	11.358
16		0.80	2.00			0.03005	9.425
17		0.80	2.25			0.03111	8.169
18		0.80	2.50			0.03307	7.184
19		0.81		10		0.03831	5.259
20		0.80		20		0.02645	12.392
21		0.80		40		0.01401	32.836
22		0.81		50		0.01052	50.686
23		0.81		60		0.00833	61.388
24		0.80		70		0.00644	84.316
25		0.80		80		0.00521	88.298
26		0.80		90		0.00394	134.559
27		0.80		100		0.00359	174.420
28		0.81			15	0.01636	22.441
29		0.80			20	0.01476	22.373
30		0.80			25	0.01279	21.725
31		0.80			50	0.00853	21.691
32		0.80			75	0.00642	21.944
33	1.00	0.80			15	0.01984	18.844
34	1.00	0.80			20	0.01713	17.402
35	1.00	0.80			25	0.01489	17.186
36	1.00	0.80			50	0.00967	17.944
37	1.00	0.80			75	0.00674	19.239
38	1.30	0.80			15	0.02401	13.340
39	1.30	0.80			20	0.01985	13.244
40	1.30	0.80			25	0.01786	13.424
41	1.30	0.80			50	0.01049	14.644
42	1.30	0.80			75	0.00773	13.765

43			0.81	0.25		15	0.00526	107.881
44			0.81	0.25		20	0.00514	107.452
45			0.81	0.25		25	0.00476	110.885
46			0.80	0.25		50	0.00403	101.094
47			0.80	0.25		75	0.00338	107.178
48			0.80	2.50		15	0.02609	7.318
49			0.80	2.50		20	0.02134	7.695
50			0.80	2.50		25	0.01843	7.620
51			0.80	2.50		50	0.01062	8.450
52	0.79		0.80	2.50		75	0.00722	7.892
53	0.79		0.80		10	15	0.02922	5.388
54	0.79		0.80		10	20	0.02328	5.268
55	0.79		0.80		10	25	0.01965	5.433
56	0.79		0.80		10	50	0.01094	6.130
57	0.79		0.80		10	75	0.00748	5.520
58			0.80		100	15	0.00343	173.528
59			0.80		100	20	0.00321	158.409
60			0.80		100	25	0.00325	152.951
61			0.80		100	50	0.00300	163.039
62			0.80		100	75	0.00256	174.058
63	0.85	0.04	0.80				0.00836	20.803
64	0.85	0.06	0.80				0.01204	20.403
65	0.85	0.08	0.80				0.01628	20.458
66	0.85	0.12	0.80				0.02360	20.548
67	0.85	0.14	0.80				0.02841	20.323
68	0.85	0.16	0.80				0.03162	20.795
69	1.20	0.04	0.80				0.01053	15.354
70	1.20	0.06	0.81				0.01598	13.550
71	1.20	0.08	0.81				0.02077	15.157
72	1.20	0.12	0.81				0.03153	14.754

73	1.20	0.14	0.81		0.03685	13.855
74	1.20	0.16	0.81		0.04235	14.683
75			0.81	0.5	0.00683	77.124
76			0.81	1.0	0.01264	37.883
77			0.81	1.5	0.01677	28.314
78			0.80	2.5	0.02073	18.497
79			0.81	5.0	0.02346	15.482
80			0.80	7.5	0.02364	14.437
81			0.80	10	0.02274	15.447
82			0.80	15	0.02153	17.841
83			0.81	25	0.01828	22.723
84			0.81	50	0.01157	42.811
85			0.80	75	0.00819	62.876
86			0.81	100	0.00643	87.765
87			0.69		0.01468	16.606
88			0.71		0.01525	18.085
89			0.73		0.01596	18.743
90			0.75		0.01680	18.747
91			0.77		0.01705	20.989
92			0.79		0.01835	19.936
93			0.82		0.02011	21.181
94			0.85		0.02109	22.837
95			0.86		0.02166	21.789
96			0.88		0.02288	23.678
97	1.30		0.08		0.00345	3.855
98	1.30		0.12		0.00505	3.531
99	1.30		0.16		0.00656	4.276
100	1.30		0.21		0.00761	4.401
101	1.30		0.27		0.00893	4.450
102	1.30		0.33		0.00939	5.690

103	1.30	0.39	0.01089	6.625
104	1.30	0.45	0.01193	7.746
105	1.30	0.51	0.01329	8.573
106	1.30	0.56	0.01473	9.514
107	1.30	0.61	0.01647	10.392
108	1.30	0.65	0.01899	11.872
109	1.30	0.71	0.02114	12.961
110	1.30	0.76	0.02387	13.124
111	1.30	0.85	0.03274	14.000
112	1.30	0.90	0.03632	14.709
113	1.30	0.95	0.04062	13.998

Table II gives an overview of the simulations carried out in this study and also reports the simulation results for the sampled heat flux q and the Kapitza length L_{K}. In total, 113 simulations were carried out. Simulation 1 (see first column in Table II) is defined as the *default simulation*. The parameters of the default simulation were chosen such that they are in the middle of the studied parametric ranges and similar to cases that were studied in the literature[3,5,9–11,33,41,42,50,53,59]. The temperature of the fluid T_{f}, the solid-fluid interaction energy $\varepsilon_{\mathrm{sf}}$, and the solid-solid interaction energy $\varepsilon_{\mathrm{ss}}$ were varied separately in the ranges $0.8 \leq T_{\mathrm{f}} \leq 1.3$, $0.25 \leq \varepsilon_{\mathrm{sf}} \leq 2.5$, and $10 \leq \varepsilon_{\mathrm{ss}} \leq 100$, while the other parameters were kept constant, i.e. their values are identical to those from the default simulation. Such single parametric variations were carried out in simulations 2 – 27. In simulations 28 – 62, the effect of the channel width H was studied with either the maximum or the minimum value of each of the three influencing factors $\varepsilon_{\mathrm{sf}}$, $\varepsilon_{\mathrm{ss}}$, and T_{f}. The channel width H was varied between 10 and 75. In simulations 1 – 62, the temperature difference between the walls and the fluid temperature in the middle of the channel was always $\Delta T_{\mathrm{w}} = 0.1$. In order to study the influence of the temperature difference ΔT_{w}, simulations with different wall temperatures were carried out for the two fluid temperatures 0.85 and 1.20 (cf. Table II, simulations 63 – 74) to generate ΔT_{w} in the range of 0.04 and 0.16. The mass of the solid particles M_{s} was varied in simulations 75 – 86 in the range $0.5 \leq M_{\mathrm{s}} \leq 100$, while the other simulation

parameters were set to the default values of simulation 1. In the remaining simulations 87 – 113, the fluid density was varied along the two isotherms $T_\mathrm{f} = 0.8$ and 1.3. The critical temperature of the LJTS fluid is at approximately $T = 1.1$[37]. Hence, the isotherm $T_\mathrm{f} = 0.8$ is in the subcritical liquid region, whereas the isotherm $T_\mathrm{f} = 1.3$ is in the supercritical region. For the supercritical isotherm ($T_\mathrm{f} = 1.3$), simulations with fluid bulk densities in the range $\rho_\mathrm{f} = 0.08$ and 0.96 were carried out. For the subcritical isotherm ($T_\mathrm{f} = 0.8$), the density was varied in the liquid state region ($0.69 \leq \rho_\mathrm{f} \leq 0.89$). Simulations with lower density have also been carried out in preliminary tests, but showed a phase separation, i.e. vapour bubbles in the metastable vapour-liquid region. The resulting state points sampled are shown in Fig. 3. Only simulation results with a homogeneous fluid bulk phase are reported here.

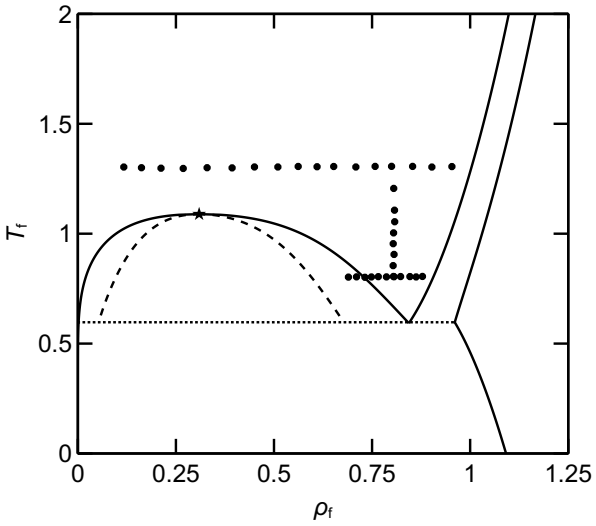

FIG. 3. Representation of the studied state points of the fluid. The filled black circles represent the simulated state points (•). The binodal and the spinodal for the vapor-liquid equilibrium of the LJTS fluid were computed from an equation of state[40]. The other phase boundaries (the sublimation, melting, and freezing line) were adopted from LJ potential data[60]. The critical point is marked by a star (⋆). The dotted line indicates the triple point temperature[37].

V. RESULTS AND DISCUSSION

A. Empirical Correlation for the Kapitza Length L_K

The results obtained from varying ΔT_w and H show that these two simulation parameters have no significant influence on the Kapitza length L_K. More information is given in the Supplementary Material. Hence, the Kapitza length L_K is discussed in the following as a function of five variables $L_K = L_K(\varepsilon_{sf}, \varepsilon_{ss}, M_s, T_f, \rho_f)$. The results presented in Table II were used to develop a simple empirical correlation, which describes the Kapitza length L_K as function of the solid-fluid interaction energy ε_{sf}, the solid-solid interaction energy ε_{ss}, the mass of the solid particles M_s, the fluid temperature T_f, and the fluid density ρ_f. The mathematical form of the empirical correlation is

$$L_K = \alpha + \beta \, (T_f \, \varepsilon_{sf})^{\gamma} \, \varepsilon_{ss}^{\delta} \, \frac{\epsilon M_s^2 + \zeta}{M_s} \, \rho_f^{(\eta T_f + \theta)}. \tag{5}$$

The numeric values of the parameters α, β, γ, δ, ϵ, ζ, η, and θ are given in Table III. The correlation yields an absolute average deviation (AAD) of 5.1% to the data used for the fit.

Eq. (5) in connection with Table III reveals that the Kapitza length L_K increases with decreasing fluid temperature T_f and decreasing solid-fluid interaction ε_{sf}. In contrast, increasing the solid-solid interaction energy ε_{ss} and increasing the density of the fluid ρ_f results in an increase of the Kapitza length L_K. A more complex behaviour is found for the dependency on M_s: the Kapitza length passes through a minimum in the studied range M_s. In the following sections, the individual influencing factors are discussed in detail.

Fig. 4 shows the performance of the empirical model (cf. Eq. 5) in a parity plot in comparison to the simulation results. For most data points, the model describes the simulation results with a relative deviation of 10% or less. Especially for moderate to high values of the Kapitza length ($10 < L_{K,sim} < 100$) where many data points are available, the correlation provides a good fit to the simulation results. For smaller values of the Kapitza length, there are more outliers. Nevertheless, most data points in this region have a relative deviation smaller than 10%.

TABLE III. Numeric values of the empirical correlation model for the Kapitza length (cf. Eq. (5)).

Parameter	Value
α	2.447
β	0.324
γ	-1.238
δ	1.781
ϵ	0.00635
ζ	0.267
η	-0.621
θ	2.057

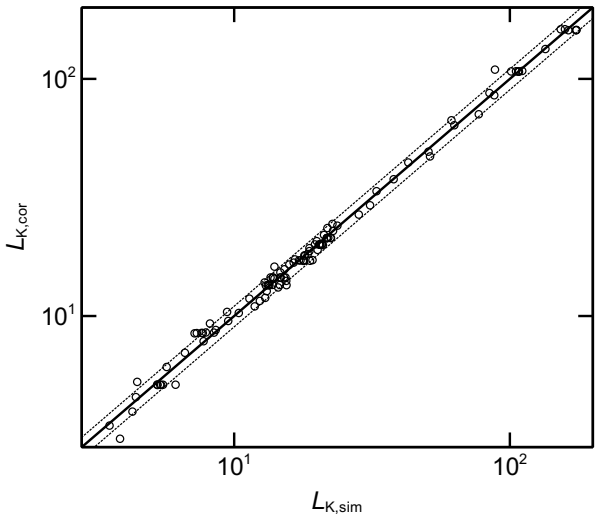

FIG. 4. Parity plot of the Kapitza length calculated from the empirical correlation (cf. Eq. 5) $L_{\mathrm{K,cor}}$ plotted over the simulation results $L_{\mathrm{K,sim}}$. Both axis have a log scale. Symbols indicate the simulation results. The black solid line represents the case $L_{\mathrm{K,cor}} = L_{\mathrm{K,sim}}$. The dotted lines represent deviations $\pm 10\%$.

B. Influence of Solid-Fluid Interaction Energy

The solid-fluid interaction energy is known to have a strong influence on the microscopic heat transfer at solid-fluid interfaces[26,29,38,41]. Fig. 5 shows the results obtained in present work for the Kapitza length as a function of the solid-fluid interaction energy $\varepsilon_{\mathrm{sf}}$ in the

simulations 1 and 10 – 18 (cf. Table II). As the solid-fluid interaction energy $\varepsilon_{\mathrm{sf}}$ increases, the Kapitza length L_{K} decreases, i.e. the transport resistance at the interface decreases. Hence, a strong solid-fluid interaction and thereby a strong coupling enables a high heat transfer across the solid-fluid interface, as expected. This is due to a stronger attractive coupling of the solid and fluid particles at the interface, which enables a better transfer of kinetic energy across the interface. For small values of the solid-fluid interaction energy, the Kapitza length exhibits large values, which is due to the repulsive interactions dominating the interactions at the interface, which acts as a hindrance for heat transfer. As the attractive interactions at the interface become important (with increasing $\varepsilon_{\mathrm{sf}}$), the dependence of the Kapitza length on $\varepsilon_{\mathrm{sf}}$ becomes weaker and the curve flattens (cf. Fig. 5). Similar observations for the dependency on the solid-fluid interaction energy were also observed for tribological properties of the same LJTS model system studied in scratching simulations[38], i.e. a strong influence of the solid-fluid interaction energy for $\varepsilon_{\mathrm{sf}} < 1$ and only a moderate influence for $\varepsilon_{\mathrm{sf}} > 1$.

Furthermore, the influence of $\varepsilon_{\mathrm{sf}}$ on the adsorption layer, which describes the layering structure at the interface, was investigated. As shown in a previous study of our group[41], the adsorption layer may have an important influence on interfacial processes. The results for the adsorption layer are presented and discussed in the Supplementary Material.

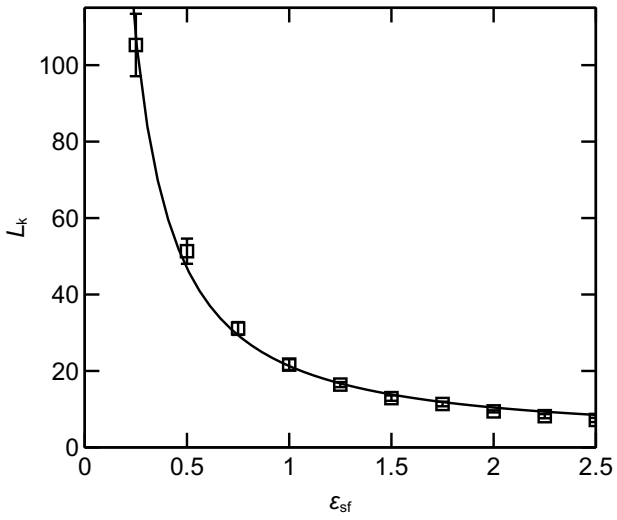

FIG. 5. Kapitza length L_K as a function of solid-fluid interaction energy ε_{sf}. Results from simulations 1 and 10 – 18 (symbols) (cf. Table II). The solid line indicates the empirical correlation (Eq. 5). For all shown data points, the simulation parameters ε_{ss}, M_s, T_f, ΔT_w, ρ_f, and H were constant (cf. Table II).

C. Influence of Solid-Solid Interaction Energy

Fig. 6 shows the Kapitza length L_K as a function of the solid-solid interaction energy ε_{ss} as obtained from simulations 1 and 19 – 27 (cf. Table II). Within the studied range, the Kapitza length L_K increases with increasing ε_{ss}. This is in accordance with the acoustic mismatch model (AMM), which predicts a deterioration of the energy transport between a solid and a fluid phase as a result of a mismatch between the solid and fluid interaction energies[2,61]. Moreover, according to the AMM, a linear relation between the misfit and the heat transfer resistance is expected. In contrast, the simulation results depicted in Fig. 6 show a non-linear relation – especially for small ε_{ss} values. This behaviour is in line with findings from studies, which showed partial failure of AMM for predicting the interfacial thermal resistance[5,9].

For large values of ε_{ss}, the heat transfer between the solid and the fluid basically breaks down; the AMM predicts: $L_K \to \infty$ for $\varepsilon_{ss} \to \infty$[2,62]. In principle, one could expect that for $\varepsilon_{ss} \to 1$ the Kapitza length $L_K \to 0$. However, this would require that also all other differences between the solid and the liquid vanish, which is not the case in the present study as the mass of the solid particles was $M_s = 2$ in simulations 19 – 27. The influence of M_s

on the results is the subject of the next section.

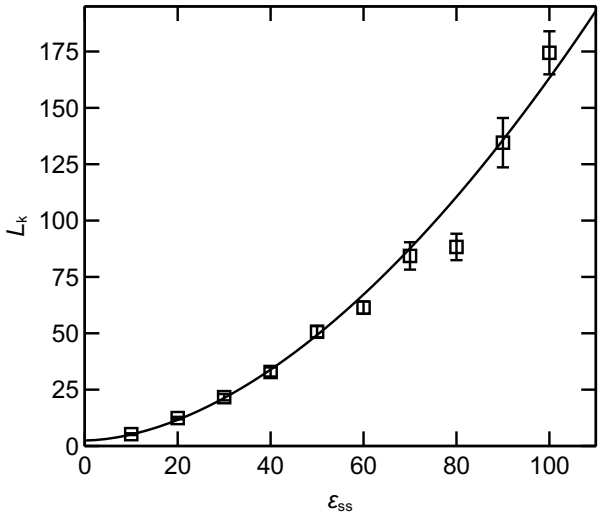

FIG. 6. Kapitza length L_K as a function of the solid-solid interaction energy ε_{ss}. Results from simulations 1 and 19 – 27 (symbols) (cf. Table II). The solid line indicates the empirical correlation (Eq. 5). For all shown data points, the simulation parameters ε_{sf}, M_s, T_f, ΔT_w, ρ_f, and H were constant (cf. Table II).

D. Influence of Mass of Solid Particles

The influence of the mass of the solid particles M_s was studied by simulations 75 – 86. The range $0.5 \leq M_s \leq 100$ covers also extreme mass ratios to investigate the limits of the Kapitza length. For $M_s < 0.5$ and $M_s > 100$, the heat flux is close to zero, which leads to large statistical uncertainties for the sampled Kapitza length. Therefore, only simulations in the range $0.5 \leq M_s \leq 100$ were included in the study. In Fig. 7, the results for the variation of M_s are shown.

The Kapitza length L_K exhibits a minimum at approximately $M_s = 7.5$. For larger masses of the solid particles, the Kapitza length increases, which is covered well by the correlation (cf. Eq. 5). According to AMM, a linear dependency of L_K on the elastic properties of the solid[2], i.e. M_s, is expected, which is confirmed by our simulations only for $M_s > 15$. At about $M_s = 7$, the Kapitza length has a minimum of about $L_K = 13$. For smaller values, the Kapitza length L_K increases with decreasing mass of the solid particles. This behaviour is a result of the decreasing momentum of the solid particles and, therefore, the decreasing

energy being transferred between solid and fluid particles when they collide. The correlation (cf. Eq. 5) describes the complex dependence of the Kapitza length on the mass of the solid particles overall well.

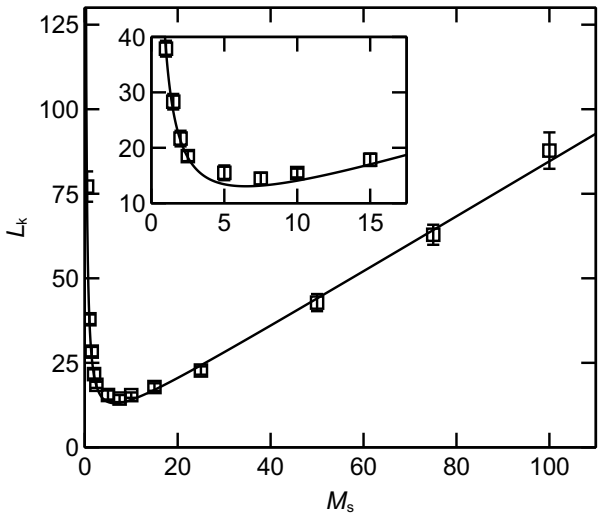

FIG. 7. Kapitza length L_K as a function of the mass of the fluid particles M_s. Results from simulations 1 and 75 – 86 (symbols) (cf. Table II). The solid line indicates the empirical correlation (Eq. 5). For all shown data points, the simulation parameters ε_{sf}, ε_{ss}, T_f, ΔT_w, ρ_f, and H were constant (cf. Table II).

E. Influence of Fluid Temperature

Fig. 8 shows the results for the Kapitza length L_K as a function of the mean fluid temperature T_f as obtained from simulations 1 – 9. In the studied temperature range, L_K decreases with increasing T_f. This qualitative behaviour of the Kapitza resistance was also reported by previous studies[10,14,26,30]. A higher mean fluid temperature T_f leads to a higher temperature of both the fluid and the solid particles in the vicinity of the interface. The effect of the fluid temperature on the structuring of the adsorption layer is shown and discussed in detail in the Supplementary Material. In general, the structuring of the adsorption layer can have an influence on the local transport properties of fluids[63,64]. However, it was found that the effective transport properties averaged across the entire adsorption layer exhibit only minor deviations from the corresponding bulk phase values[41] for systems as the ones studied here.

With increasing temperature, the mean undirected kinetic energy of the particles and thus their mobility increases, which yields higher collision rates in both, bulk phases and at the interface, which decreases interfacial heat transfer resistance and thereby the Kapitza length. The Fluid structure at the interface (see Supplementary Material) becomes less prominent with increasing temperature, which counteracts the aforementioned effect. As the interfacial structuring of the fluid decreases with increasing temperature, both phases become more unlike and fewer fluid particles are permanently coupled to solid-phase particles at the interface. This hinders the heat transfer through the interface and is also in accordance with AMM[2]. In the simulation results from this work, the temperature effect on the overall particle mobility dominates the adverse effect from the adsorption structure. Yet, even for the highest temperature (which is slightly above the critical point of the LJTS fluid[35]) studied here, the Kapitza length L_K remains fairly high.

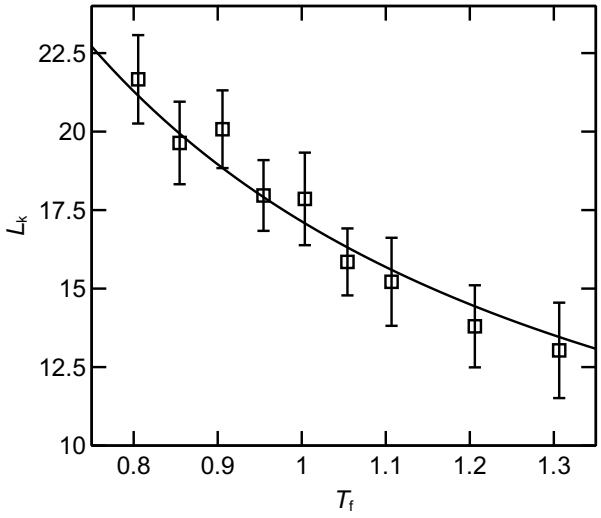

FIG. 8. Kapitza length L_K as a function of the fluid temperature T_f. Results from simulations 1 – 9 (symbols) (cf. Table II). The solid line indicates the empirical correlation (Eq. 5). For all shown data points, the simulation parameters ε_sf, ε_ss, M_s, ΔT_w, ρ_f, and H were constant (cf. Table II).

F. Influence of Fluid Density

The influence of the fluid density ρ_f was studied in the liquid phase region ($T_\mathrm{f} = 0.8$) and at supercritical conditions ($T_\mathrm{f} = 1.3$, cf. Fig. 3). The corresponding simulation results are shown in Fig. 9. For both isotherms, the Kapitza length L_K increases monotonically

with increasing fluid density. Such behavior was already reported by Amani et al.[26] for liquid phase state points. The results for $T_\mathrm{f} = 1.3$ show that this also holds at supercritical conditions and for low densities of the fluid. Yet, the density dependence is found to be more prominent at low temperatures, i.e. the slope of $L_\mathrm{K}(\rho_\mathrm{f})$ is larger at low temperatures. Moreover, it can be seen that the influence of temperature and density on L_K plays an important role. The developed empirical correlation describes the behavior well for both, the sub- and the supercritical temperature.

An increasing Kapitza length with increasing fluid density may be considered counter-intuitive: one might expect an improvement of the heat transfer as the particles bump into each other more often at higher densities. This would lead to larger transfer of momentum between the solid and the fluid particles and, therefore, decrease the interfacial heat resistance. However, this mechanism is counteracted by an increasing structuring in adsorption layers with increasing density and an increasing dominance of repulsive interactions. The adsorption layers are shown in the Supplementary Materials for ten state points with $0.08 \leq \rho_\mathrm{f} \leq 0.96$ and $T_\mathrm{f} = 1.3$. With increasing density, the number of adsorption layers increases, while the individual layers become thinner at the same time. This leads to a decrease of the mobility of the particles in the vicinity of the interface, especially perpendicular to the surface, and thereby also to an increase of the interfacial heat resistance.

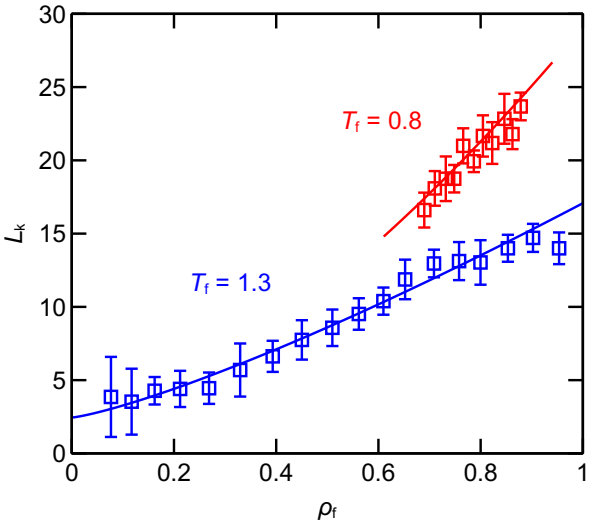

FIG. 9. Kapitza length L_K as a function of the fluid density ρ_f for the temperatures $T_f = 0.8$ (red) and $T_f = 1.3$ (blue). Results from simulations 1 and 87 – 113 (symbols), (cf. Table II). The solid lines indicate the empirical correlation (Eq. 5). For all shown data points, the simulation parameters ε_{sf}, ε_{ss}, M_s, ΔT_w and H were constant (cf. Table II).

G. Introducing the Kapitza Interface Number *Ki* for Modeling the Heat Transfer

In the heat transfer simulation scenario studied here (cf. Fig. 1), heat conduction in the fluid plays an important role. Even in the case of total absence of the Kapitza effect (i.e. for $L_K = 0$), there is the heat transfer resistance due to the heat conduction in the fluid between the two planar walls, which is simply

$$R_{cond} = \frac{H}{\lambda} \ , \tag{6}$$

where H is the channel width and λ is the thermal conductivity of the fluid. Here, we assume that the mean thermal conductivity in the adsorption layer is the same as in the bulk fluid, which is a reasonable approximation, as the temperature profiles that were observed in the liquid were basically linear in all cases studied in the present work. For a systematic investigation of the thermal conductivity of the LJTS fluid near walls, see Ref.[41].

It is, therefore, interesting to relate the Kapitza heat transfer resistance R_K, which is

simply

$$R_{\mathrm{K}} = \frac{L_{\mathrm{K}}}{\lambda} \tag{7}$$

to R_{cond}. The quotient $R_{\mathrm{K}}/R_{\mathrm{cond}}$ is a dimensionless number, which we call Kapitza interface number Ki. It follows from Eq. (6) and (7) that

$$Ki = \frac{R_{\mathrm{K}}}{R_{\mathrm{cond}}} = \frac{L_{\mathrm{K}}}{H} \ , \tag{8}$$

which gives a descriptive geometric interpretation of Ki as the ratio of the Kapitza length L_{K} and the characteristic macroscopic length of the problem, which is H here.

The total thermal resistance R_{total} in a system without convection, as it was considered in this work, is defined as the sum of the conductive thermal resistance R_{cond} and the Kapitza resistance R_{K}

$$R_{\mathrm{total}} = R_{\mathrm{K}} + R_{\mathrm{cond}} = \frac{H}{\lambda}\left(Ki + 1\right) \ . \tag{9}$$

Here, the conductive thermal resistance of the walls is neglected and a constant wall temperature is assumed (cf. Fig. 2). For the LJTS system studied here, this is an excellent assumption due to the much higher thermal conductivity in the solid compared to the fluid[33,65].

The dimensionless number Ki characterizes the influence of the Kapitza interface resistance on the total thermal resistance. Due to its definition (see Eq. 8), Ki goes to zero for large channel widths H, and the influence of the Kapitza resistance on the total heat transfer resistance R_{tot} vanishes, see Eq. (9). Fig. 10 shows the dependency of the results for the Ki number obtained from the simulations of the present work on the channel width H. As expected, Ki decreases inversely proportional to H, which indicates that the numbers for L_{K} are independent of the channel width H, which is also shown in the Supplementary Material and is in line with findings from the literature[19,20]. As can be seen in Fig. 10, the empirical correlation developed in this work agrees well with the simulation results. Only for simulations 19 and 53 – 57 ($\triangleleft$) with weak solid-solid interaction energies and, therefore, small values for the Kapitza length L_{K} (cf. section V C), the correlation shows some deviations from the simulation results as already discussed in section V A. Fig. 10 illustrates that the dimensionless number Ki is particularly high for weak solid-fluid interaction energies $\varepsilon_{\mathrm{sf}}$ ($\triangle$) and large solid-solid interaction energies $\varepsilon_{\mathrm{ss}}$ ($\triangleright$). For both simulation series ($\triangle$ and $\triangleright$),

$Ki > 1$ holds for all conducted simulations. In Fig. 10, the results from the correlation are deliberately shown for a very large range of H covering values up to 1000, which is much higher than the maximum channel width studied here, which was about $H_{\max} = 75$. Values of $Ki > 1$ indicate that the Kapitza resistance R_K is larger than the resistance due to heat conductivity R_{cond}, but even for $Ki = 0.1$ the Kapitza resistance R_K is 10% of R_{cond}, and hence, not negligible. Fig. 10 illustrates that this is true in many cases even for channel widths as large as 2000 molecular diameters ($H = 1000$).

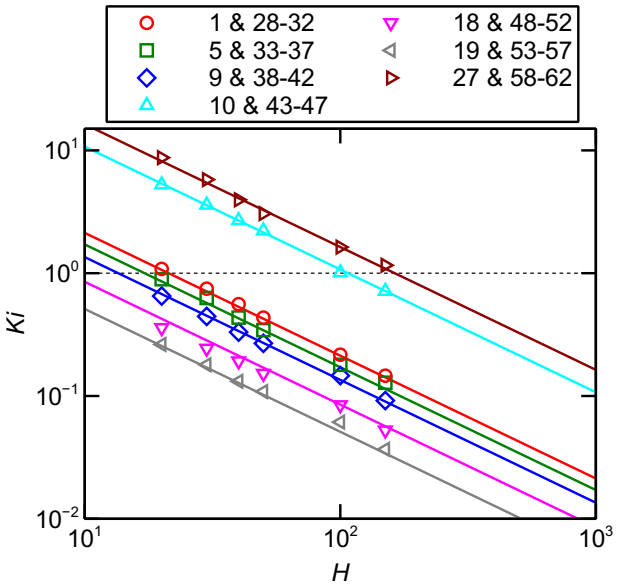

FIG. 10. Kapitza interface number Ki as function of the channel width H as log-log plot. Symbols indicate simulation results; the numbers given in the legend correspond to the simulation numbers given in Table II. The solid lines represent the values for Ki obtained from the empirical correlation for L_K (Eq. (5) and Eq. (8)).

H. Application of *Ki* for Describing Heat Transfer with Convection and Scale-up of the Results

In general, the application of the correlation given in Eq. (5) on real substance systems requires the estimation of the parameters, which describe the molecular interactions and the size of the molecules, namely ε_{ff}, ε_{sf}, ε_{ss}, and σ_{ff}. These parameters can be estimated by different methods. For the parameters of the fluid ε_{ff} and σ_{ff}, there are many parameter

sets given in the literature, mainly for small, spherical molecules[47,66]. Estimations for the solid-solid interaction energy $\varepsilon_{\mathrm{ss}}$ are also available for different materials, e.g. for some metals[67]. The solid-fluid interaction energy $\varepsilon_{\mathrm{sf}}$ can be derived from the wetting behavior of the material pairing[36]. With these four parameters given, all quantities involved in a given problem (e.g. T or H) can be reduced (cf. Table I) and the correlation in conjunction with Eq. (8) can be used to estimate Ki. Merabia et al.[68] showed that such a mapping of results from a Lennard-Jones model system to real systems of nanoparticles based on a corresponding states principle yields good results.

In the following, it is briefly discussed, how the results for Ki that were obtained in the present work can be applied for describing heat transfer with convection. Also the scale-up from nanoscale channels to macroscale channels is discussed. As an example, the following situation is considered: a fluid flows between two parallel planar walls of the temperature T_{w}, which differs from the fluid temperature T_{f}, which is defined here as the temperature of the fluid in the middle of the channel for the sake of simplicity. The characteristic length L of such a scenario is usually defined in terms of the channel width, i.e. $L = 2H$[69,70]. The Kapitza interface number Ki (cf. Eq. (8)) accounts for the Kapitza resistance in the absence of convection.

The heat transfer from a solid surface with the temperature T_{w} to a bulk fluid with the temperature T_{f} is described by

$$q = \frac{T_{\mathrm{w}} - T_{\mathrm{f}}}{R_{\mathrm{total}}} \ , \tag{10}$$

where R_{total} is the total thermal resistance, which can be written as

$$R_{\mathrm{total}} = R_{\mathrm{K}} + R_{\mathrm{conv}} \ . \tag{11}$$

The term R_{conv} includes the convective and the conductive contribution to the thermal resistance such that Eq. (9) is extended to systems with convection. The summation of the resistances in Eq. (11) is adapted from Refs.[71–73]. Usually, the transport resistance R_{conv} is calculated in engineering from the Nusselt number Nu:

$$R_{\mathrm{conv}} = \frac{1}{\alpha_{\mathrm{conv}}} = \frac{L}{Nu\ \lambda} = \frac{2\ H}{Nu\ \lambda} \ , \tag{12}$$

where α_{conv} is the convective heat transfer coefficient. From Eqs. (8), (11), and (12), it follows that

$$R_{\mathrm{total}} = \frac{H}{\lambda}\left(Ki + \frac{2}{Nu}\right) \ . \tag{13}$$

Eq. (13) accounts for the interfacial resistance, the conductive, and convective heat transfer effects. Heat conduction in the flowing bulk fluid is incorporated in the Nusselt number Nu. Different Nusselt number correlations have been proposed in the literature[74], which may yield different limits for zero flow velocity. In many cases, the limit is zero, i.e. heat conduction is neglected. To be consistent with the discussion above, the limit of the Nusselt number for zero flow velocity should be $Nu = 2$ (cf. Eq. 9 and 13).

Eq. (13) also enables discussing the influence of the scale of the problem on the heat transfer. The scale is determined by the geometric parameter H. As H increases, Ki approaches 0 and the right side of Eq. (13) is dominated by Nu. On the other side, for small H, $Ki \gg 1$ and there is a significant contribution of the term Ki to the total heat transfer resistance. Fig. 10 shows that, even for a simple fluid as studied in this work, the contribution from Ki may play a role up to $H = 1000$. For a fairly small organic molecule with $\sigma = 0.5$ nm this corresponds to $H = 0.5$ µm. This is only a ballpark estimate. The correlation presented in Eq. (5) enables more accurate considerations for specific situations.

VI. CONCLUSIONS

In this work, the heat transfer across a solid-fluid interface was studied in a model system using molecular dynamics simulations. In the simulation scenario, a stagnant fluid was confined between two planar fixed walls with different temperatures. The heat transfer resistance between the two thermostatted walls can be split up in a formal way into two contributions: firstly, a resistance that would be present if the entire channel was filled with the stagnant bulk fluid, and secondly, a contribution that accounts for the heat transfer resistance at the interfaces, which is known as the Kapitza resistance and usually characterized by the Kapitza length.

We studied a model system, where both the fluid and the wall particles were described with the Lennard-Jones truncated and shifted potential. The influence of different parameters on the heat transfer was studied systematically: the strength of the solid-fluid

interaction, the strength of the solid-solid interaction, the mass of the solid particles, the fluid density, the fluid temperature, the temperature difference between solid and fluid as well as the channel width. The obtained results for the dependencies of the Kapitza length L_K on these parameters were correlated by a simple analytical function. The temperature of the wall and the channel width were found to have no significant influence on the interfacial heat transfer resistance. For the fluid temperature T_f, an increasing T_f yields a decreasing interfacial heat transfer resistance. Furthermore, a strong mismatch between the solid-solid interaction and the fluid-fluid interaction energies leads to a high heat transfer resistance at the interface, while a strong solid-fluid interaction decreases that resistance. These findings are in line with results reported in the literature[4,9,10,26,31]. An increase of the fluid density leads to an increase of the Kapitza length for both studied temperatures, the subcritical and the supercritical isotherms. For liquid states, this behavior was also reported by Amani et al.[26]. The mass of the solid particles has a more complex influence on the interfacial heat transfer resistance: the Kapitza length exhibits a minimum as a function of the mass of the solid particles. The Kapitza length is found to be minimal for a reduced mass of the solid particles of about $M_\mathrm{s} \approx 7.5$. For future work, it would be interesting to analyze the different contributions to the heat flux, i.e. the kinetic and the configurational contributions[75,76], in the adsorption layer to elucidate different mechanisms in detail.

Furthermore, the study yields information on the scale of the problem. The influence of the interfacial thermal resistance and the bulk fluid thermal resistance of the heat transfer can readily be estimated using the dimensionless number proposed in this work. For large scales, the heat transfer is dominated by heat conduction and the Kapitza resistance is negligible. But as the scale becomes smaller, the influence of the Kapitza resistance increases. It can play a role in channels with widths corresponding to several hundred diameters of the fluid molecules. The results of our study provide a simple yet effective tool to estimate the relevance of the interfacial heat transfer resistance in a given heat transfer problem.

ACKNOWLEDGMENTS

The project was funded by the Deutsche Forschungsgemeinschaft (DFG, German Research Foundation) – 252408385 – IRTG 2057 *Physical Modeling for Virtual Manufacturing Systems and Processes* and – Project-ID 172116086 – SFB 926 *Microscale Morphology of*

Component Surfaces as well as by the Federal Ministry of Education and Research (BMBF, Germany) – 01IH16008 – *Task-based load balancing and auto-tuning in particle simulations* (TaLPas). The simulations were carried out on the HazelHen at High Performance Computing Center Stuttgart (HLRS) under the grant MMHBF2, on *elwe* at Regional University Computing Center Kaiserslautern (RHRK) under the grant TUK-TLMV as well as on the SuperMuc at Leibniz Supercomputing Center (LRZ) Garching under the grant SPARLAMPE (pr48te). The present research was conducted under the auspices of the Boltzmann-Zuse Society for Computational Molecular Engineering (BZS).

REFERENCES

[1]P. L. Kapitza, "The study of heat transfer in helium II," Journal of Physics (USSR) **4**, 181 (1941).

[2]G. L. Pollack, "Kapitza Resistance," Reviews of Modern Physics **41**, 48–81 (1969).

[3]M. R. Hasan, T. Q. Vo, and B. Kim, "Manipulating thermal resistance at the solid–fluid interface through monolayer deposition," RSC Advances **9**, 4948–4956 (2019).

[4]M. Barisik and A. Beskok, "Temperature dependence of thermal resistance at the water/silicon interface," International Journal of Thermal Sciences **77**, 47–54 (2014).

[5]B. H. Kim, A. Beskok, and T. Cagin, "Molecular dynamics simulations of thermal resistance at the liquid-solid interface," The Journal of Chemical Physics **129**, 174701 (2008).

[6]T. Q. Vo and B. Kim, "Interface thermal resistance between liquid water and various metallic surfaces," International Journal of Precision Engineering and Manufacturing **16**, 1341–1346 (2015).

[7]T. Q. Vo and B. Kim, "Transport phenomena of water in molecular fluidic channels," Scientific Reports **6**, 33881 (2016).

[8]T. Q. Vo and B. Kim, "Physical origins of temperature continuity at an interface between a crystal and its melt," The Journal of Chemical Physics **148**, 034703 (2018).

[9]L. Xue, P. Keblinski, S. Phillpot, S.-S. Choi, and J. Eastman, "Two regimes of thermal resistance at a liquid–solid interface," The Journal of Chemical Physics **118**, 337–339 (2003).

[10]G. Song and C. Min, "Temperature dependence of thermal resistance at a solid/liquid interface," Molecular Physics **111**, 903–908 (2013).

[11]R. Khare, P. Keblinski, and A. Yethiraj, "Molecular dynamics simulations of heat and momentum transfer at a solid–fluid interface: relationship between thermal and velocity slip," International Journal of Heat and Mass Transfer **49**, 3401–3407 (2006).

[12]S. Alosious, S. K. Kannam, S. P. Sathian, and B. D. Todd, "Nanoconfinement effects on the kapitza resistance at water–CNT interfaces," Langmuir **37**, 2355–2361 (2021).

[13]Z. Liang, K. Sasikumar, and P. Keblinski, "Thermal transport across a substrate–thin-film interface: Effects of film thickness and surface roughness," Physical Review Letters **113**, 065901 (2014).

[14]H.-C. Dan, Z.-M. Zou, Z. Zhang, and J.-W. Tan, "Effects of aggregate type and SBS copolymer on the interfacial heat transport ability of asphalt mixture using molecular dynamics simulation," Construction and Building Materials **250**, 118922 (2020).

[15]H. Han, C. Schlawitschek, N. Katyal, P. Stephan, T. Gambaryan-Roisman, F. Leroy, and F. Müller-Plathe, "Solid–liquid interface thermal resistance affects the evaporation rate of droplets from a surface: A study of perfluorohexane on chromium using molecular dynamics and continuum theory," Langmuir **33**, 5336–5343 (2017).

[16]A. Sarode, Z. Ahmed, P. Basarkar, A. Bhargav, and D. Banerjee, "Role of carbon nanotube on the interfacial thermal resistance: A molecular dynamics approach," *2017 16th IEEE Intersociety Conference on Thermal and Thermomechanical Phenomena in Electronic Systems (ITherm)*, (2017), 10.1109/ITHERM.2017.7992493.

[17]J. Vera and Y. Bayazitoglu, "Temperature and heat flux dependence of thermal resistance of water/metal nanoparticle interfaces at sub-boiling temperatures," International Journal of Heat and Mass Transfer **86**, 433–442 (2015).

[18]A. T. Pham, M. Barisik, and B. Kim, "Interfacial thermal resistance between the graphene-coated copper and liquid water," International Journal of Heat and Mass Transfer **97**, 422–431 (2016).

[19]S. Alosious, S. K. Kannam, S. P. Sathian, and B. D. Todd, "Kapitza resistance at water–graphene interfaces," The Journal of Chemical Physics **152**, 224703 (2020).

[20]D. Alexeev, J. Chen, J. H. Walther, K. P. Giapis, P. Angelikopoulos, and P. Koumoutsakos, "Kapitza resistance between few-layer graphene and water: Liquid layering effects," Nano Letters **15**, 5744–5749 (2015).

[21]H. Hu and Y. Sun, "Effect of nanopatterns on Kapitza resistance at a water-gold interface during boiling: A molecular dynamics study," Journal of Applied Physics **112**, 053508

(2012).

[22]A. T. Pham, M. Barisik, and B. Kim, "Molecular dynamics simulations of Kapitza length for argon-silicon and water-silicon interfaces," International Journal of Precision Engineering and Manufacturing **15**, 323–329 (2014).

[23]Z.-Y. Ong, "Thickness-dependent Kapitza resistance in multilayered graphene and other two-dimensional crystals," Physical Review B **95**, 155309 (2017).

[24]D. Ghatage, G. Tomar, and R. K. Shukla, "Thermostat-induced spurious interfacial resistance in non-equilibrium molecular dynamics simulations of solid–liquid and solid–solid systems," The Journal of Chemical Physics **153**, 164110 (2020).

[25]A. Pham, M. Barisik, and B. Kim, "Pressure dependence of Kapitza resistance at gold/water and silicon/water interfaces," The Journal of Chemical Physics **139**, 244702 (2013).

[26]A. Amani, S. M. H. Karimian, and M. Seyednia, "A molecular dynamics simulation on the effect of different parameters on thermal resistance of graphene-argon interface," Molecular Simulation **43**, 276–283 (2016).

[27]Z. H. Kou, M. L. Bai, and G. C. Zhao, "Molecular dynamics simulations of thermal transport at the nanoscale solid-liquid interface," Applied Mechanics and Materials **291-294**, 1999–2003 (2013).

[28]S. Murad and I. K. Puri, "Molecular simulation of thermal transport across hydrophilic interfaces," Chemical Physics Letters **467**, 110–113 (2008).

[29]F. Jabbari, A. Rajabpour, S. Saedodin, and S. Wongwises, "Effect of water/carbon interaction strength on interfacial thermal resistance and the surrounding molecular nanolayer of CNT and graphene flake," Journal of Molecular Liquids **282**, 197–204 (2019).

[30]A. France-Lanord, P. Soukiassian, C. Glattli, and E. Wimmer, "Ab initio parameterization of a charge optimized many-body forcefield for Si–SiO2: Validation and thermal transport in nanostructures," The Journal of Chemical Physics **144**, 104705 (2016).

[31]S. Ge and M. Chen, "Vibrational coupling and kapitza resistance at a solid–liquid interface," International Journal of Thermophysics **34**, 64–77 (2013).

[32]M. Heier, S. Stephan, J. Liu, W. G. Chapman, H. Hasse, and K. Langenbach, "Equation of state for the Lennard-Jones truncated and shifted fluid with a cut-off radius of 2.5 σ based on perturbation theory and its applications to interfacial thermodynamics," Molecular Physics **116**, 2083–2094 (2018).

[33]M. P. Lautenschlaeger and H. Hasse, "Transport properties of the Lennard-Jones truncated and shifted fluid from non-equilibrium molecular dynamics simulations," Fluid Phase Equilibria **482**, 38–47 (2019).

[34]K. R. S. Shaul, A. J. Schultz, and D. A. Kofke, "The effect of truncation and shift on virial coefficients of Lennard-Jones potentials," Collection of Czechoslovak Chemical Communications **75**, 447–462 (2010).

[35]S. Stephan, J. Liu, K. Langenbach, W. G. Chapman, and H. Hasse, "Vapor-liquid interface of the Lennard-Jones truncated and shifted fluid: Comparison of molecular simulation, density gradient theory, and density functional theory," The Journal of Physical Chemistry C **122**, 24705–24715 (2018).

[36]S. Becker, H. M. Urbassek, M. T. Horsch, and H. Hasse, "Contact angle of sessile drops in Lennard-Jones systems," Langmuir **30**, 13606–13614 (2014).

[37]S. Stephan and H. Hasse, "Influence of dispersive long-range interactions on properties of vapour-liquid equilibria and interfaces of binary Lennard-Jones mixtures," Molecular Physics **118**, e1699185 (2020).

[38]S. Stephan, M. Dyga, H. Urbassek, and H. Hasse, "The influence of lubrication and the solid-fluid interaction on thermodynamic properties in a nanoscopic scratching process," Langmuir **35**, 16948–16960 (2019).

[39]F. Diewald, M. Lautenschlaeger, S. Stephan, K. Langenbach, C. Kuhn, S. Seckler, H.-J. Bungartz, H. Hasse, and R. Müller, "Molecular dynamics and phase field simulations of droplets on surfaces with wettability gradient," Computer Methods in Applied Mechanics and Engineering **361**, 112773 (2020).

[40]M. Heier, F. Diewald, M. T. Horsch, K. Langenbach, R. Müller, and H. Hasse, "Molecular dynamics study of adsorption of the Lennard-Jones truncated and shifted fluid on planar walls," Journal of Chemical & Engineering Data **64**, 386–394 (2019).

[41]M. P. Lautenschlaeger and H. Hasse, "Thermal, caloric and transport properties of the Lennard-Jones truncated and shifted fluid in the adsorbed layers at dispersive solid walls," Molecular Physics **118**, 1–10 (2019).

[42]M. P. Lautenschlaeger, S. Stephan, M. T. Horsch, B. Kirsch, J. C. Aurich, and H. Hasse, "Effects of lubrication on friction and heat transfer in machining processes on the nanoscale: A molecular dynamics approach," Procedia CIRP **67**, 296–301 (2018).

[43]J. Liu, M. Heier, W. G. Chapman, and K. Langenbach, "Adsorption in purely dispersive

systems from molecular simulation, density gradient theory, and density functional theory," Journal of Chemical & Engineering Data **65**, 1222–1233 (2020).

[44]S. Stephan, D. Schaefer, K. Langenbach, and H. Hasse, "Mass transfer through vapour-liquid interfaces: A molecular dynamics simulation study," Molecular Physics **119**, e1810798 (2020).

[45]M. P. Lautenschlaeger, M. T. Horsch, and H. Hasse, "Simultaneous determination of thermal conductivity and shear viscosity using two-gradient non-equilibrium molecular dynamics simulations," Molecular Physics **117**, 189–199 (2019).

[46]S. Schmitt, S. Stephan, B. Kirsch, J. C. Aurich, E. Kerscher, H. M. Urbassek, and H. Hasse, "Molecular Simulation Study on the Influence of the Scratching Velocity on Nanoscopic Contact Processes," in *2nd International Conference of the DFG International Research Training Group 2057 – Physical Modeling for Virtual Manufacturing (iPMVM 2020)*, Open Access Series in Informatics (OASIcs), Vol. 89 (Dagstuhl, Germany, 2021) pp. 17:1–17:16.

[47]S. Stephan, M. T. Horsch, J. Vrabec, and H. Hasse, "MolMod - an open access database of force fields for molecular simulations of fluids," Molecular Simulation **45**, 806–814 (2019).

[48]I. Mudawwar and M. El-Masri, "Momentum and heat transfer across freely-falling turbulent liquid films," International Journal of Multiphase Flow **12**, 771–790 (1986).

[49]D. C. Marable, S. Shin, and A. Y. Nobakht, "Investigation into the microscopic mechanisms influencing convective heat transfer of water flow in graphene nanochannels," International Journal of Heat and Mass Transfer **109**, 28–39 (2017).

[50]S. Ge, Y. Gu, and M. Chen, "A molecular dynamics simulation on the convective heat transfer in nanochannels," Molecular Physics **113**, 703–710 (2015).

[51]A. Pellew and R. V. Southwell, "On maintained convective motion in a fluid heated from below," Proceedings of the Royal Society of London. Series A. Mathematical and Physical Sciences **176**, 312–343 (1940).

[52]S. Plimpton, "Fast parallel algorithms for short-range molecular dynamics," Journal of Computational Physics **117**, 1–19 (1995).

[53]Y. Akkus, C. T. Nguyen, A. T. Celebi, and A. Beskok, "A first look at the performance of nano-grooved heat pipes," International Journal of Heat and Mass Transfer **132**, 280–287 (2019).

[54]Q. Van Dinh, T. Q. Vo, and B. Kim, "Viscous heating and temperature profiles of liquid water flows in copper nanochannel," Journal of Mechanical Science and Technology **33**,

3257–3263 (2019).

[55]C. T. Nguyen, M. Barisik, and B. Kim, "Wetting of chemically heterogeneous striped surfaces: Molecular dynamics simulations," AIP Advances **8**, 065003 (2018).

[56]J. Ghorbanian and A. Beskok, "Scale effects in nano-channel liquid flows," Microfluidics and Nanofluidics **20**, 121 (2016).

[57]Y. Noh, T. Vo, and B. Kim, "Subatomic-level solid/fluid boundary of Lennard-Jones atoms: A molecular dynamics study of metal-inert fluid interface," Applied Sciences **9**, 2439 (2019).

[58]M. Heier, S. Stephan, F. Diewald, R. Müller, K. Langenbach, and H. Hasse, "Molecular Dynamics Study of Wetting and Adsorption of Binary Mixtures of the Lennard-Jones Truncated and Shifted Fluid on a Planar Wall," Langmuir **37**, 7405–7419 (2021).

[59]M. P. Lautenschlaeger and H. Hasse, "Thermal and caloric properties of fluids from non-equilibrium molecular dynamics simulations using the two-gradient method," The Journal of Chemical Physics **149**, 244106 (2018).

[60]A. J. Schultz and D. A. Kofke, "Comprehensive high-precision high-accuracy equation of state and coexistence properties for classical Lennard-Jones crystals and low-temperature fluid phases," The Journal of Chemical Physics **149**, 204508 (2018).

[61]D. G. Cahill, W. K. Ford, K. E. Goodson, G. D. Mahan, A. Majumdar, H. J. Maris, R. Merlin, and S. R. Phillpot, "Nanoscale thermal transport," Journal of Applied Physics **93**, 793–818 (2003).

[62]S. A. Khrapak, "Sound velocities of Lennard-Jones systems near the liquid-solid phase transition," Molecules **25**, 3498 (2020).

[63]H. Hoang and G. Galliero, "Local viscosity of a fluid confined in a narrow pore," Physical Review E **86**, 021202 (2012).

[64]I. Bitsanis and G. Hadziioannou, "Molecular dynamics simulations of the structure and dynamics of confined polymer melts," The Journal of Chemical Physics **92**, 3827–3847 (1990).

[65]S. Volz, J.-B. Saulnier, M. Lallemand, B. Perrin, P. Depondt, and M. Mareschal, "Transient Fourier-law deviation by molecular dynamics in solid argon," Physical Review B **54**, 340–347 (1996).

[66]J. Vrabec, G. K. Kedia, G. Fuchs, and H. Hasse, "Comprehensive study of the vapour–liquid coexistence of the truncated and shifted Lennard–Jones fluid including planar and spherical interface properties," Molecular Physics **104**, 1509–1527 (2006).

[67]T. Halicioğlu and G. M. Pound, "Calculation of potential energy parameters from crystalline state properties," Physica Status Solidi (a) **30**, 619–623 (1975).

[68]S. Merabia, S. Shenogin, L. Joly, P. Keblinski, and J.-L. Barrat, "Heat transfer from nanoparticles: A corresponding state analysis," Proceedings of the National Academy of Sciences **106**, 15113–15118 (2009).

[69]D. Nield, A. Kuznetsov, and M. Xiong, "Thermally developing forced convection in a porous medium: parallel plate channel with walls at uniform temperature, with axial conduction and viscous dissipation effects," International Journal of Heat and Mass Transfer **46**, 643–651 (2003).

[70]D. A. Nield, A. Bejan, *et al.*, *Convection in porous media*, Vol. 3 (Springer, New York, 2006).

[71]D. Dai, Y. Zhou, and J. Liu, "Liquid metal based thermoelectric generation system for waste heat recovery," Renewable Energy **36**, 3530–3536 (2011).

[72]D. B. Tuckerman and R. F. W. Pease, "High-performance heat sinking for VLSI," IEEE Electron device letters **2**, 126–129 (1981).

[73]T.-H. Tsai and R. Chein, "Performance analysis of nanofluid-cooled microchannel heat sinks," International Journal of Heat and Fluid Flow **28**, 1013–1026 (2007).

[74]J. P. Holman, *Heat transfer*, 10th ed., McGraw-Hill series in mechanical engineering (McGraw Hill Higher Education, Boston, 2010).

[75]M. H. Ernst, E. H. Hauge, and J. M. J. van Leeuwen, "Asymptotic time behavior of correlation functions. II. Kinetic and potential terms," Journal of Statistical Physics **15**, 7–22 (1976).

[76]G. Galliero and C. Boned, "Thermal conductivity of the Lennard-Jones chain fluid model," Physical Review E **80**, 061202 (2009).